IEEE Access
Multidisciplinary | Rapid Review | Open Access Journal

Received November 5, 2020, accepted November 22, 2020, date of publication November 30, 2020,
date of current version December 15, 2020.

Digital Object Identifier 10.1109/ACCESS.2020.3041232

3D-Printed Low-Profile Single-Substrate Multi-Metal Layer Antennas and Array With Bandwidth Enhancement

MENGZE LI[1], (Student Member, IEEE), YANG YANG[1], (Senior Member, IEEE), FRANCESCA IACOPI[1,2], (Senior Member, IEEE), JAIM NULMAN[3], (Senior Member, IEEE), AND SHLOMIT CHAPPEL-RAM[3]

[1]School of Electrical and Data Engineering, University of Technology Sydney, Sydney, NSW 2007, Australia
[2]Australian Research Council Centre of Excellence in Transformative Meta-Optical Systems, University of Technology Sydney, Sydney, NSW 2007, Australia
[3]Nano Dimension, Ness Ziona 7403635, Israel

Corresponding author: Yang Yang (yang.yang.au@ieee.org)

This work was supported by Nano Dimension through a Ph.D. scholarship agreement, in part by UTS ProtoSpace, and in part by the UTS FEIT Blue Sky Grant.

ABSTRACT This paper presents a few single-substrate multi-metal layer antennas using additively manufactured electronics (AME) solution based on piezoelectric additive fabrication. By vertically stacking metal layers in a 3D printed single substrate, the designed antenna prototype exhibits the advantages of wide bandwidth and ultra-low profile. For proof-of-concept, multi-layer linear polarization (LP) patch antenna elements and 2 × 2 LP antenna arrays are designed, fabricated, and measured. It verifies that the feeding network can be integrated into the same substrate of the antenna array element without increasing the size and profile of the array. Compared with the traditional single-layer LP patch antenna, the proposed LP patch antenna can improve the impedance bandwidth from 5.9% to 10.6% (three layers) and 83% (seven layers), respectively. All these designs can be fabricated in a single substrate with a thickness of 1.5 mm (0.031 λ_g), which is an ideal solution for the applications where ultra-low profile and wideband patch antenna are expected. Finally, circular polarization (CP) patch antenna elements and 2 × 2 CP antenna arrays are fabricated and measured. Good agreements between the simulated and the measured results verify that wider impedance bandwidth and broader frequency range of under 3-dB axial ratio can be obtained by vertically stacking metal layers. The antennas are designed at sub-6GHz, which have great potentials for 5G consumer mobile electronics.

INDEX TERMS Additive manufacture, 3D printing technology, wideband antennas, multi-metal layer antennas, sub-6GHz, 5G, consumer electronics.

I. INTRODUCTION

Additive manufacturing (AM) is a potential game-changer that may completely overset the manufacturing value chain in Industry 4.0. In the electronics industry, AM technology has the advantages of low cost, fast prototyping, three-dimensional (3D) customized design freedom, and a distributed production circle. 3D printing is an alternative method to replace or complement traditional fabrication. Many complex systems, which are difficult to implement using conventional fabrication methods, can be prototyped and realized.

According to the open literature, 3D printed electronic components have been achieved in types of waveguides [1], reflectarrays [2], [3], lenses, [4], transmitarray [5], frequency selective surfaces [6], [7], transmission lines (TLs) [8], [9], filters [10], and antennas [11]–[41]. Most of these applied AM approaches are based on printing the entire geometry with a single material printer, such as metal/dielectric 3D printers [1], [2], or loading metallic paint with metal casting 3D printers on different kinds of substrates, for example, textiles [11] or papers [12], [14]. It is often difficult to utilize these single material printing processes to handle advanced

The associate editor coordinating the review of this manuscript and approving it for publication was Chow-Yen-Desmond Sim.

designs with complex structures composed of conductive and dielectric parts in a single substrate. This is particularly challenging when the high-conductive and dielectric materials need to be fully integrated using a single-substrate 3D printer, which often requires more steps and additional processing time during fabrication [16]. Moreover, it is difficult to fabricate multi-layer structures using conventional single-material AM technology [17]. Fortunately, the advancement of AM technology has recently produced a new generation of 3D printing techniques and materials that can fabricate conductor and dielectric simultaneously [9,], [10], [42], [43].

In this paper, a novel AME method is proposed for designing ultralow profile single-substrate wideband antennas and arrays. Multi-metal layers are seamlessly printed in a single substrate to excite additional resonate modes that can be controlled independently. With the increase of stacked patches, the impedance bandwidth can rise from 5.9% (single layer) to 10.6% (three layers) and 83% (seven layers), respectively, without increasing the total profile of the antenna. Furthermore, taking advantage of AME, the feeding network is integrated into the same substrate of the antenna array elements without increasing the size and profile of the array. The electrical properties of this 3D printing material are investigated at 3.6 GHz using an embedded transmission line (TL). Then, a three-layer LP antenna element and a 2×2 LP array are seamlessly printed into single-substrate, respectively. Furthermore, the multi-layer circular polarization (CP) antennas are investigated for wide impedance bandwidth and 3-dB ratio axial by stacking patches in a single thin substrate. According to the open literature, the proposed designs are believed to be one of the lowest profiled patch antennas, with wideband performance.

The rest of this paper is organized as follows. Section II presents the fabrication process and proposed AME solution. Section III shows the dielectric property characterization for the desired frequency region by analyzing the transmission line models. Section IV presents the multi-Layer LP antennas and array design, and evaluation using the simulated and measured results. Section V offers the multi-Layer CP antennas and array design, followed by Section VI that concludes the paper.

II. PROPOSED ADDITIVELY MANUFACTURED ELECTRONICS SOLUTION

A. PROCESS AND PROTOTYPING

Fig. 1 shows the composition of the 3D printing system, in which two print heads have 512 nozzles for conductive and dielectric ink jetting, respectively. An infrared radiation (IR) lamp with a wavelength of 0.75-1.4 μm and 140°C to 170°C process temperature is used to sinter the conductive ink. An ultraviolet (UV) lamp with a wavelength of 395 nm is used to cure the dielectric ink. The printing process is carried out at a typical temperature of 140°C in a standard ambient atmosphere. Conveniently, multiple prototype samples can be produced at one time.

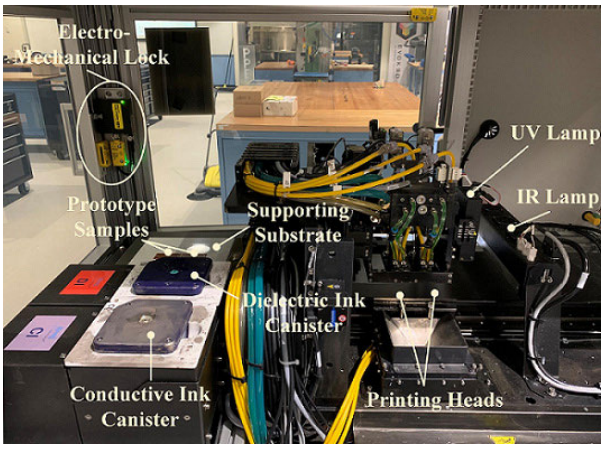

FIGURE 1. 3D printing system using fully-integrated dielectric and conductive inks.

Current commonly used 3D manufacturing technologies can be classified into three main groups: continuous liquid interface production (CLIP), material jetting (InkJet), and selective laser sintering (SLS) [44]. As a kind of inkjet, the AME approach uses piezoelectric based nozzles with deposition of liquid ink. For piezoelectric 3D printing, an applied voltage generates a pressure pulse in the fluid to force a droplet of ink from the nozzle. As shown in Fig. 2a, when the magnitude of the applied voltage raised high enough to a threshold voltage, inks will be pressed from the nozzles. Compared with thermal inkjet technology, piezo inkjet allows a wider variety of inks, since a volatile component is not required.

Fig. 2b depicts the fabrication guidelines for the proposed 3D printing solution:

1) Step 1 - a bottom solder mask is printed for soldering purposes. A plated through-hole is printed at the same time.

2) Step 2 - the designed circuit, consisting of conductor and dielectric, is built on top of the solder mask layer with the hole extended through the dielectric layer. To help us understand the flow chart, close-up views of the fabricated plated through-holes and traces are shown in Fig. 2b as well (steps 1 and 2 above).

3) Step 3 - a pure dielectric layer is built, including vias and through holes.

4) Step 4 - another circuit layer is printed in both conductor and dielectric inks, where the vias and through holes link multiple layers.

5) Step 5 - a pure dielectric layer is built with the through-holes kept extending.

6) Step 6 - the finishing of the multilayer process by coating an additional solder mask.

Note that by repeating the process of fabrication of conductive and dielectric layers (Steps 2 to 5), multilayer components can be produced, provided that the total thickness of the printed prototype meets the design rule of less than 3 mm. This fully-integrated solution has the advantage of seamlessly printing complex 3D prototypes composed of both dielectric and conductive materials. Double-sided, multilayer circuits

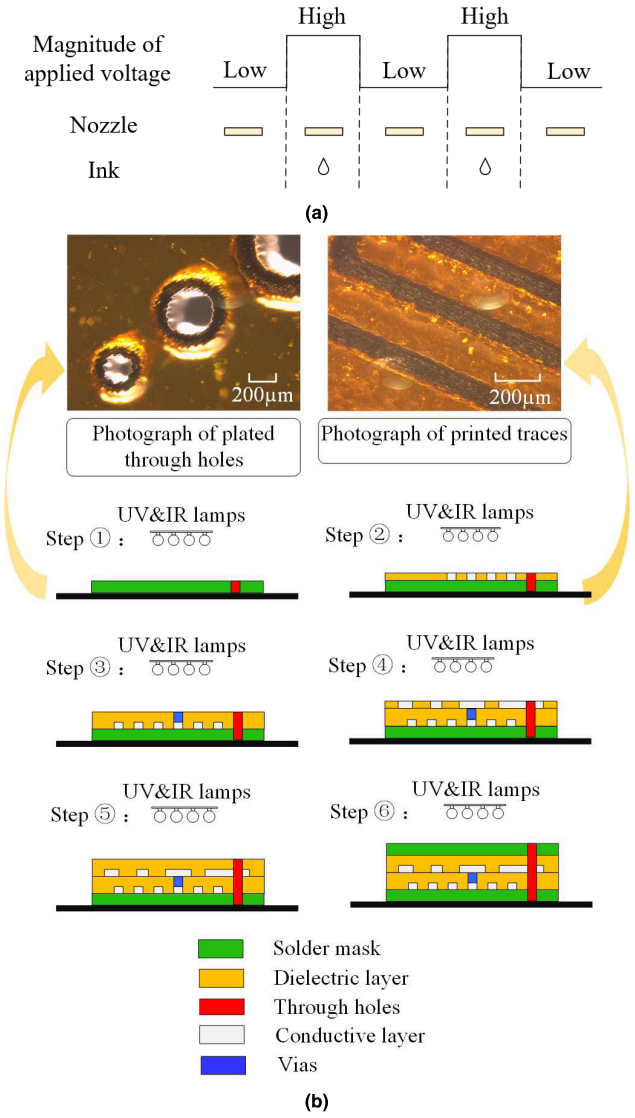

FIGURE 2. (a) Working diagram of piezoelectric inkjet. (b) Flow chart of fabrication process using the fully integrated AME system, including photographs of printed plated through holes and traces.

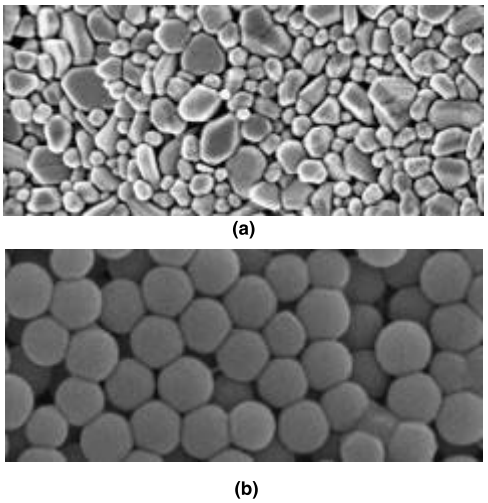

FIGURE 3. Photos of (a) AgCite nano-Silver ink and (b) Acrylates, used by the AME system.

TABLE 1. Dielectric properties, Dk and Df as function of frequency in the 200 MHz to 20 GHz range.

Frequency (GHz)	0.2	0.5	1	2
ϵ'	2.9	2.83	2.81	2.79
$tan(\delta)$	0.079	0.049	0.037	0.026
Frequency (GHz)	5	10	15	20
ϵ'	2.75	2.74	2.73	2.69
$tan(\delta)$	0.019	0.023	0.016	0.008

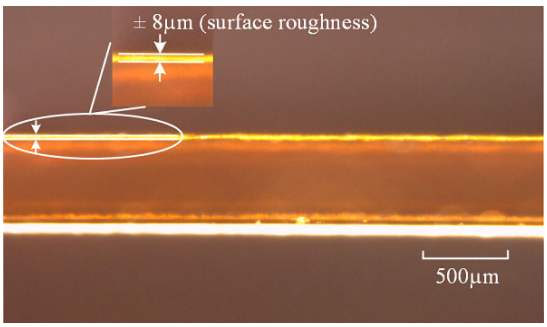

FIGURE 4. Photograph of the printed substrate – across-section view.

with through holes, plated through-holes, or vias with good radio frequency (RF) quality can be fabricated. Photograph of plated through holes and traces are depicted in Fig. 2b as well.

B. MATERIALS AND PRECISION

As illustrated in Figs. 3a and 3b, the conductive ink (AgCite^{TM} nano-silver), and the dielectric ink (acrylate) used by the inkjet system, have tightly-controlled particle sizes and excellent stability for precision AM tasks. In particular, the inks have unique and compatible sintering and curing properties. The dielectric formulation yields unique electrical properties in terms of loss tangent and dielectric constant, as listed in Table 1.

Fig. 4 shows a photograph of the printed substrate in a cross-sectional view. The variation of surface smoothness is $\pm$ 8 μm within the scan range of 1 mm length. The printer can print boards up to 160 $\times$ 160 $\times$ 3 mm^3. The design rule is specified as 110 μm in traces, 110 μm in spaces and a minimum layer thickness of 0.3μ m and 2.5 μm for the conductive layer and a dielectric layer, respectively. This specification allows the machine to meet the demanding design and quality requirements of industries, such as healthcare and aerospace, where microscale precision manufacturing is expected.

III. ANALYSIS OF 3D PRINTED TRANSMISSION LINES

To investigate the electrical properties of the 3D printing dielectric materials for loss analysis, an embedded TL with acrylate as the substrate material is analyzed and discussed.

As shown in Fig. 5a, the conductive metal for signal transmission is embedded in the dielectric medium, and a_1, a_2, and b_1, b_2 denote the widths and lengths of the surface soldering

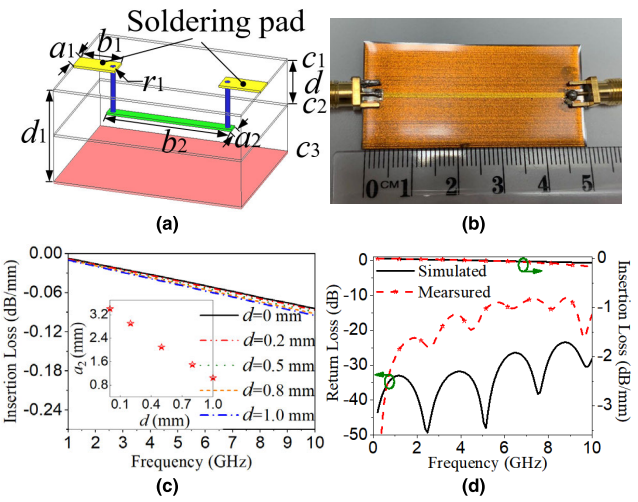

FIGURE 5. (a) Layout of embedded TL, (b) Photograph of fabricated embedded TL, (c) Transmission coefficients of the embedded TL with varying d; the inset figure shows the values of a_2 and d to keep a 50 Ω characteristic impedance. (d) Simulated and measured insertion loss and return loss for embedded TL. For $a_1 = 2.6$, $a_2 = 1.1$, $b_1 = 3$, $b_2 = 44$, $c_1 = c_2 = c_3 = 0.02$, $d = 0.5$, $d_1 = 1$, $r_1 = 0.25$ (Unit: mm).

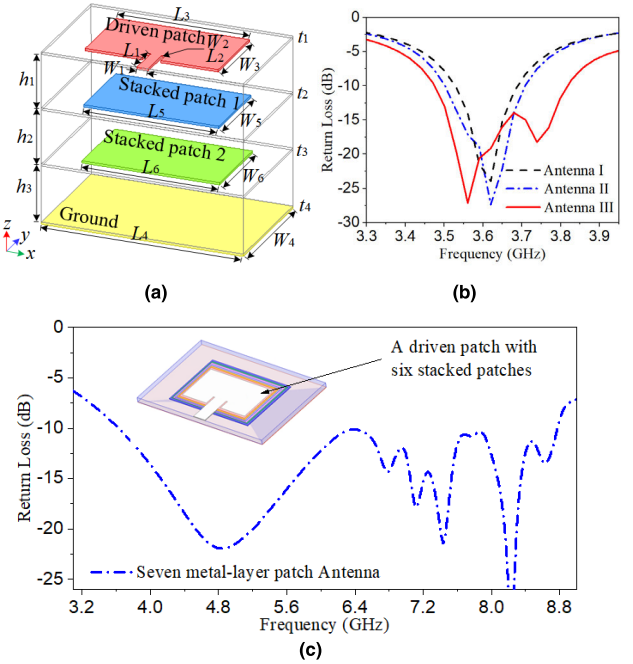

FIGURE 6. Layouts of (a) Antenna I - patch antenna with stacked patches 1 and 2, and the simulated return loss of (b) Antenna I, Antenna II and Antenna III. (c) Simulated return loss of seven-layer patch antenna with its layout embedded. ($L_1 = 12$, $L_2 = 5$, $L_3 = 38$, $L_4 = 59$, $L_5 = 39$, $L_6 = 60$, $W_1 = 4.9$, $W = 0.5$, $W_3 = 22.6$, $W_4 = 36.6$, $W_5 = 23.1$, $W_6 = 23.3$, $h_1 = 0.28$, $h_2 = 0.78$, $h_3 = 0.36$, $t_1 = t_2 = t_3 = t_4 = 0.02$. (Unit: mm)).

pad and embedded TL, respectively. In addition, the surface soldering pad and embedded TL are connected by vias, the radius of which is r_1, c_1, c_2, and c_3 are the thicknesses of metal layers, d represents the depth of the transmission line embedded in the acrylate substrate, and d_1 is the thickness of the dielectric substrate. The photograph of fabricated TL model is depicted in Fig. 5b.

As Fig. 5c shows, the transmission coefficient tends to degrade slightly as the embedded line is pushed into the substrate further away from the top surface. In order to maintain the required impedance match, the embedded TLs are set at 50 Ω, which can be adjusted by the value of a_2, as shown in the inset of Fig. 5c. Finally, a sample with $d = 1$ mm is simulated, fabricated, and measured, as shown in Fig. 5d. The TL printed in the depth of 1.0 mm shows a maximum insertion loss of 0.03 dB/mm at 3.5 GHz and 0.09 dB/mm at 10 GHz. The differences between simulated and experimental results are due to the connection loss of the SMA connectors, of which the cut-off frequency is lower than 10 GHz.

IV. MULTI-LAYER LINEAR POLARIZATION ANTENNAS AND ANTENNA ARRAY

A. MULTILAYER LINEAR POLARIZATION ANTENNAS

Figs. 6a demonstrates the layout of Antenna I, which is a three-layer patch antenna consisting of a driven patch and two stacked patches. To verify the radiation performance of the 3D printed multi-layer antennas, single-layer patch antennas (Antenna I), patch antenna with stacked patch 1 (Antenna II), and patch antenna with stacked patches 1 and 2 (Antenna III), were designed and fabricated. According to Fig. 6b, an additional resonate mode can be introduced when a stacked patch is added in the antenna. Compared with Antenna I, the total −10 dB bandwidth of Antenna III rises from 5.9% to 10.6%. Moreover, As shown in Fig. 6c, when the number of stacked patches raises to six, the operational frequency band can increase to 5.14 GHz (3.63-8.77 GHz), achieving a bandwidth of 83%, with a peak gain of 1.45 dBi, while its total thickness is kept as 1.5 mm. The results indicate that adding stacked patches generates additional resonant modes to enhance the operational bandwidth, while the total profile of the substrate remains unchanged, taking advantage of multi-mode resonant characteristics. Fig. 6a gives the detailed dimensions of the three-layer patch antenna.

In addition, these resonant modes excited by stacking patches can be adjusted. Taking the three-layer antenna as an example, three resonant modes, f_1, f_2, and f_3, can be independently controlled by tuning the width of driven and stacked patches. Fig. 7a reveals that, by raising W_3 from 22.4 to 22.8 mm, f_3 can be adjusted to a lower frequency while f_1 and f_2 remain unchanged. Fig. 7b shows that, by raising W_6 from 23.6 to 24 mm, f_2 and f_3 remain constant, while f_1 decreases gradually. When adjusting the widths W_3, W_5, and W_6, simultaneously, as shown in Fig. 7c, the three resonant modes, f_1, f_2, and f_3 of the antenna can be shifted with a fixed absolute bandwidth. After optimization, Fig. 7d shows the fabricated three-layer patch antenna with the antenna gains and return loss in the comparison between simulation and measurement. Good agreement can be obtained between the simulated and measured results. The measured peak gain is 3.8 dBi at 3.5 GHz. The measured return loss lower than −10 dB is from 3.5-3.89 GHz.

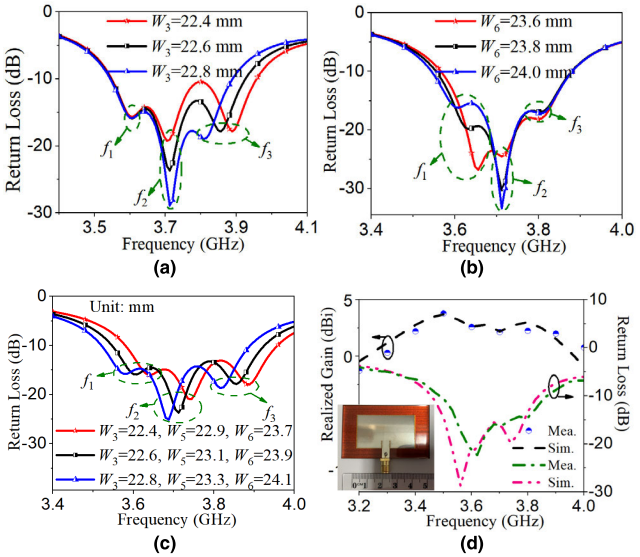

FIGURE 7. The bandwidth of three-layer patch antenna varies against (a) W_3, ($W_5 = 23.1$, $W_6 = 23.9$) (b) W_6, ($W_3 = 22.9$, $W_5 = 23.1$), (c) W_3, W_5 and W_6 and (d) Measured and simulated gains and return loss of three-layer patch antenna as well as its photograph.

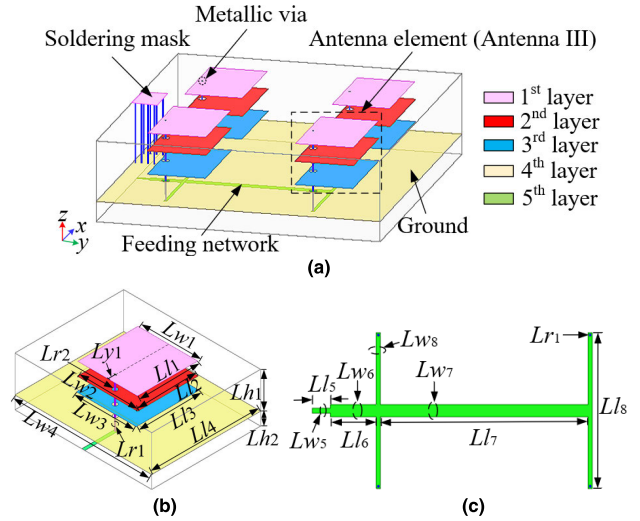

FIGURE 8. Layouts of (a) Multilayer antenna array and detail dimensions of its (b) Antenna element and (c) Feeding network. ($Ll_1 = 22.6$, $Ll_2 = 22.9$, $Ll_3 = 23.3$, $Ll_4 = 39.3$, $Ll_5 = 5$, $Ll_6 = 12.9$, $Ll_7 = 50$, $Ll_8 = 57$, $Lw_1 = 38$, $Lw_2 = 39$, $Lw_3 = 40$, $Lw_4 = 70$, $Lw_5 = 1.2$, $Lw_6 = Lw_7 = 3.3$, $Lw_8 = 1.2$, $Ly_1 = 1.05$, $Lr_1 = 0.3$, $Lr_2 = 0.5$, $Lh_1 = 1.5$, $Lh_2 = 0.5$. (Unit: mm)).

Compared with previous reported 3D printed patch antennas (see Table 2). The proposed three-layer antenna can provide wide operational bandwidth with an extremely low-profile. Moreover, since we use an integrated printing approach, no post-processing procedures are needed, which makes the design more reliable and robust.

B. MULTILAYER LP ANTENNA ARRAY

Based on the 3D printed three-layer antenna, a multi-layer LP antenna array is proposed. As shown in Fig. 8a, the configuration of the multi-layer LP antenna includes five conductive layers (three layers for antenna elements, one layer for ground and one layer for feeding network) and the

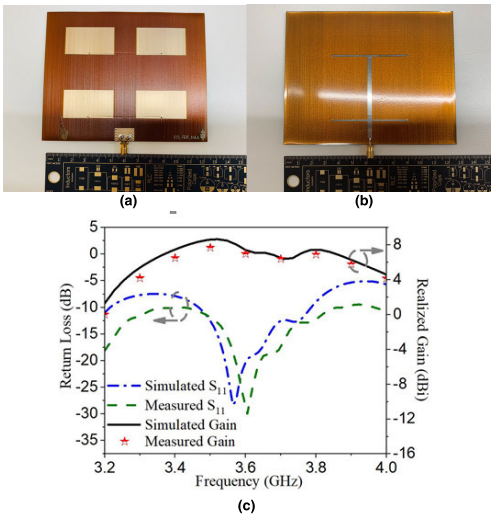

FIGURE 9. Prototypes of (a) Top view and (b) Bottom view of the multilayer antenna array. (c) Measured and simulated gains and return loss.

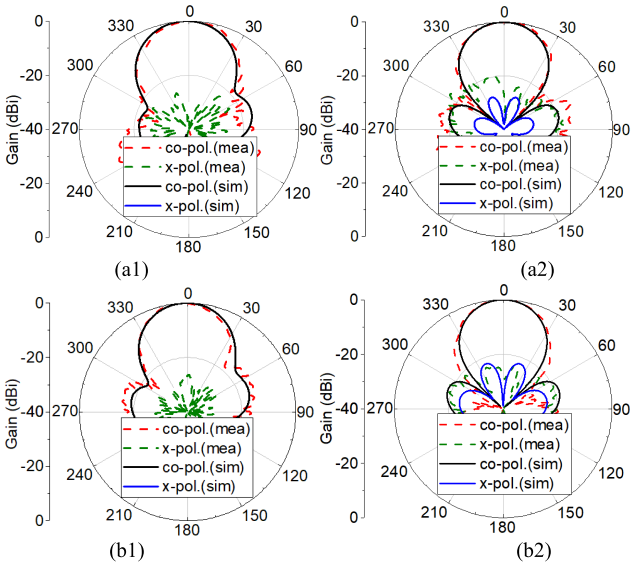

FIGURE 10. Radiation patterns of multilayer antenna array. (a1) YOZ-plane at 3.5 GHz, (a2) XOZ-plane at 3.5 GHz, (b1) YOZ-plane at 3.6 GHz, (b2) XOZ -plane at 3.6 GHz.

thickness of each conductive layer is set at 20 μm. The top three conductor layers consist of four antenna elements. The feeding network is located at the bottom layer of the substrate. A ground layer is printed between the antenna element and the feeding network. The shape and location of the feeding network have no effect on the antenna array elements on the other side of the ground, which increases the design freedom. Four metallic vias going through the stacked patches (the second and third layers) and the ground layer (the fourth layer) are introduced to connect the driven patch (the top layer) and the feeding network (the fifth layer). In addition, on the top layer, a soldering mask (10 mm $\times$ 15 mm) for welding is connected to the ground layer by eight metallic vias, whose radius is 0.3 mm. The detailed dimensions of the antenna element and feeding line are shown in Figs. 8b and 8c.

TABLE 2. Comparison with previously reported 3D printed patch antennas.

Ref.	construction	Tan (δ)	ϵ'	$^{*}f_c$ (GHz)	Gain (dBi)	-10 dB bandwidth	Size (λ_g^2)	Thickness (λ_g)	Fabricating process
This work	Single element (Three-layer patches)	0.03	2.8	3.68	3.8	10.6%	0.478×0.821	0.031	Dielectric and conductive ink integrated printing
This work	2×2 array	0.03	2.8	3.63	7.7	12.7%	1.95×1.80	0.041	Dielectric and conductive ink integrated printing
[13]	4×3 array	0.07	35	2.45	0.86	10.1%	7.25×6.28	0.150	Cooper tape +paper for dielectric part
[14]	Single patch	0.02	5.05	2.4	/	3.3%	0.323×0.504	/	Meandered and flexible silicone + copper tape
[15]	Curved single patch	0.015	2.54	2.45	6.28	9%	0.294×0.612	0.129	Curved conductive copper tape + polymer
[16]	1×4 phased array	0.005	2.7	3.5	/	3.7%	1.63×3.685	0.403	Cooper tape + polymer substrate
[17]	2×2 patch antenna array	0.047	2.96	6	4.17	/	0.909×0.929	/	Liquid-Metal-Filled patches + polymer
[18]	Single patch	0.005	2.7	1.65-2.17	$^{\#}$0.5-4.5	/	0.186×0.186	0.08	Aluminum tape + polymer
[19]	Single patch	0.01	2.7	7.5	5.5	/	0.37×0.453	0.131	Metal wire mesh + polymer
[20]	Two stacked patches	0.0253	3.11	2.75/3.2	6.7/7.3	9.4%	0.615×0.615	0.089	Copper slices + polymer slices connected with screw
[21]	Honeycomb-inspired single patch antenna	0.02	3	2.4	8.1	8.3%	0.444×0.444	0.069	Inkjet-Printed both metallic and polymer part (separated steps)

*Center Frequency; #1.5 at 1.65 GHz to 4.5 at 2.17 GHz.

The Vector Network Analyzer (VNA) used in the measurement is a Keysight PNA N5225B, and the simulation analysis software, ANSYS High-Frequency Structure Simulator (HFSS), is utilized in the simulation. A comparison with previous reported 3D printed patch antennas is detailed in Table 2. The simulated and measured results show good agreement. Figs. 9a and 9b show the top and bottom views of the fabricated antenna array. Fig. 9c shows the simulated and measured realized gains and return loss of the multi-layer antenna array. The measured peak gain is 7.7 dBi at 3.5 GHz. The measured frequency range lower than −10 dB is from 3.46−3.93 GHz. The simulated antenna efficiency is 45%. Fig. 10 depicts the simulated and measured radiation patterns of the multi-layer antenna array at 3.5 GHz and 3.6 GHz in the E-plane and H-plane, respectively.

V. MULTI-LAYER CIRCULAR POLARIZATION ANTENNAS AND ANTENNA ARRAY

A. MULTILAYER CIRCULAR POLARIZATION ANTENNAS

The circular polarization (CP) can be obtained by implementing two orthogonal modes. A common way to achieve CP is to trim the ends of two opposite corners of a square patch. As shown in Fig. 11a, single layer microstrip square-patch antenna with truncated corners are depicted and its detailed parameters are given in the index. Fig. 11b shows the simulated return loss of the single-layer CP antenna, where the excited two orthogonal modes are located at f_1 and f_2. Figs. 11c and 11d give the current distribution over the square-patch of the CP antenna at these two orthogonal modes, f_3 and f_4, respectively. As seen from Fig.11c, the direction of the current at f_3 is top left, while the direction of the current at f_4 is bottom left, as shown in Fig.11d. It verifies that introducing truncated corners on a patch antenna can help to generate two orthogonal modes, which are vertical to each other.

To further investigated this theory about multi-layer patch antennas, based on the traditional single-layer CP antenna (Antenna IV), stacked patches are added to construct the

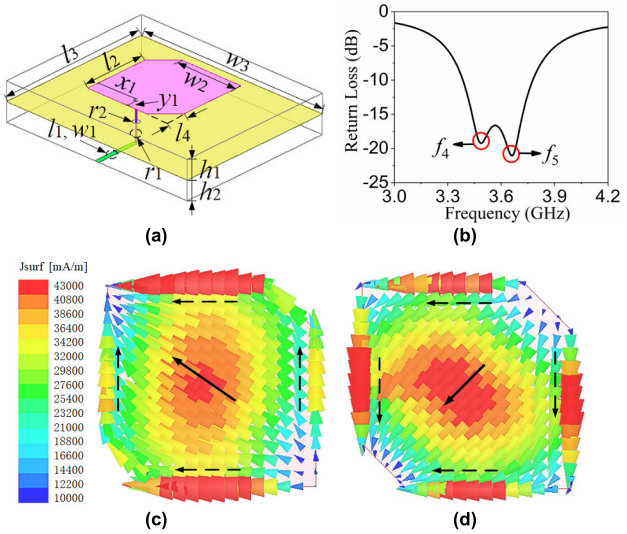

FIGURE 11. Layouts of single layer CP antenna and its (b) simulated return loss, as well as the current distribution over the antenna patch at (c) 3.48 GHz and (d) 3.66 GHz. ($l_1 = 13$, $l_2 = 19$, $l_3 = 42.4$, $l_4 = 5.2$, $w_1 = 1.2$, $w_2 = 18.4$, $w_3 = 53.3$, $x_1 = 11.8$, $y_1 = 3.3$, $r_1 = 0.3$, $r_2 = 0.6$, $h_1 = 1.5$, $h_2 = 0.5$. (unit: mm)).

double-layer (Antenna V) and three-layer (Antenna VI) CP patch antennas, Fig. 12a demonstrates the layout of the three-layer patch antenna consisting of a driven patch and two stacked patches with truncated corners. Distance between the driven patch, the first added stacked patch, the second added a stacked patch, and the top of the substrate are 0 mm, 0.3 mm and 1.1 mm, respectively. Fig. 12b depicts the simulated return loss of these three CP antennas. Obviously, with the increase of the amounts of stacked patches from 0 to 2, the quantity of resonate modes improved from 2 to 6, which matches that every metal patch of the multi-layer CP antenna can excite two orthogonal modes. Furthermore, the axial ratio can also be improved with the increase of the amounts of stacked patches. As shown in Fig. 12c, from Antenna IV to Antenna VI, the minimal axial ratio is improved from 4.9 dB to 0.16 dB. The frequency range of 3-dB axial ratio is improved from 0 to 126 MHz (3.556 GHz to 3.682 GHz).

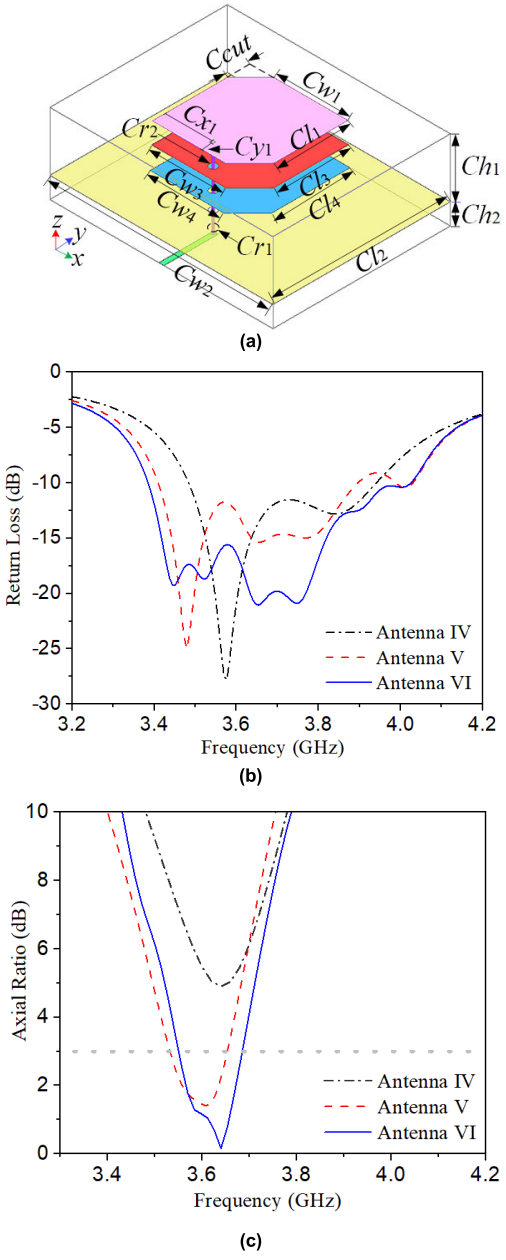

FIGURE 12. Layouts of (a) Three-layer patch antenna consisting of a driven patch and two stacked patches with truncated corners as well as (b) Simulated return loss and (c) Axial ratio of Antenna IV, Antenna V and Antenna VI. ($Cl_1 = 17.8$, $Cl_2 = 43.2$, $Cl_3 = 18$, $Cl_4 = 18.8$, $Cw_1 = 17.6$, $Cw_2 = 53.8$, $Cw_3 = 17.9$, $Cw_4 = 17.7$, $Cx_1 = 11.6$, $Cy_1 = 2.9$, $Cr_1 = 0.3$, $Cr_2 = 0.6$. $Ch_1 = 1.5$, $Ch_2 = 0.5$, $Ccut = 5.6$. (unit: mm)).

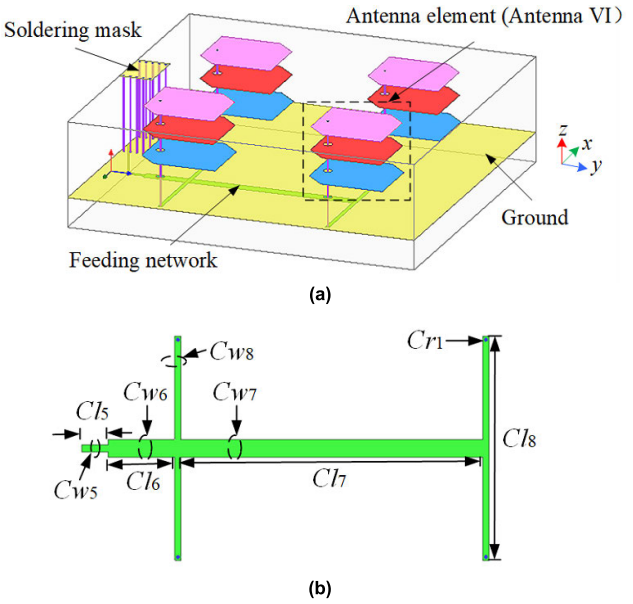

FIGURE 13. Layouts of (a) CP multilayer antenna array and detail dimensions of its (b) Feeding network. ($Ll_5 = 5$, $Ll_6 = 12$, $Ll_7 = 50$, $Ll_8 = 51.5$, $Lw_5 = 1.2$, $Lw_6 = Lw_7 = 3.3$, $Lw_8 = 1.2$, $Cr_1 = 0.3$. (unit: mm)).

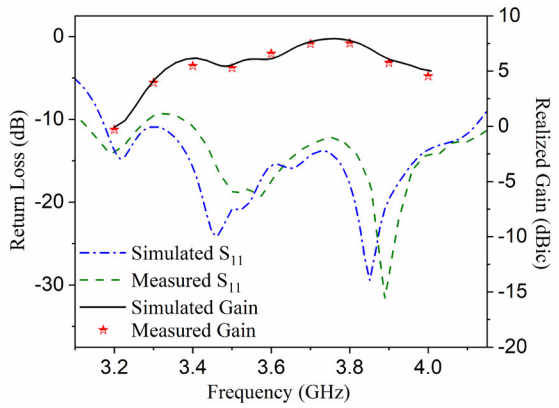

FIGURE 14. Realized gain and return loss of proposed CP multilayer antenna array.

B. MULTILAYER CIRCULAR POLARIZATION ANTENNA ARRAY

A circular polarized (CP) multi-layer antenna array is proposed based on the 3D printed three-layer antenna (Antenna VI), as shown in Fig. 13a. Like the LP multi-layer antenna array, five metal layers are introduced to construct the CP multi-layer antenna array. The thickness of metal layer is 20 μm. The detailed dimensions of these four antennas elements are the same as the Antenna VI. The feeding network is printed on the bottom surface of the substrate connected to the first patch (driven patch) of Antenna VI with metallic vias. A 10 mm × 15 mm rectangular metal mask connecting to the ground layer is designed on the top surface of the substrate for soldering. Fig. 13b depicts the detailed dimensions of the feeding network of the proposed multi-layer CP antenna array.

Finally, good agreement is reached between the simulated and measured results. Furthermore, seen from Fig. 14, which shows the simulated and measured realized gain and return loss from 3.2 GHz to 4 GHz of the multi-layer CP antenna array, the simulated peak gain is 7.6 dBic at 3.8 GHz. For the return loss, six resonate modes are achieved and the frequency range lower than −8.8 dB is from 3.1–4.17 GHz. In Fig. 15, the minimal measured axial ratio of the multi-layer CP antenna array is 1.97 dB at 3.6 GHz, and the operational range where the simulated AR is lower than 3-dBi can

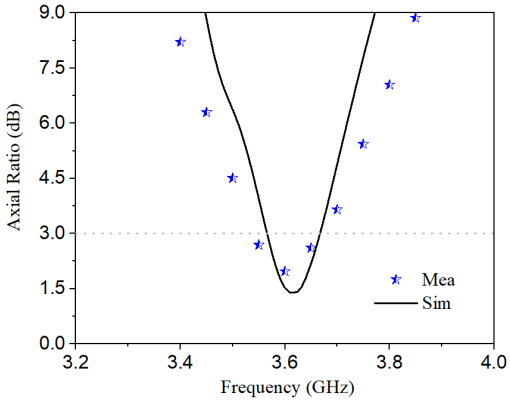

FIGURE 15. Simulated and measured axial ratio of multilayer CP antenna array.

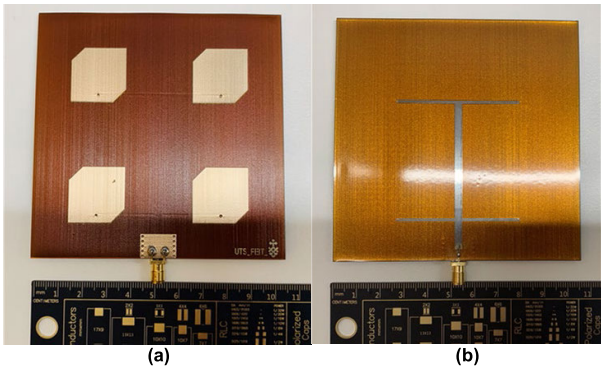

FIGURE 16. Photographs seen from (a) top view and (b) bottom view of the CP multilayer antenna array prototype.

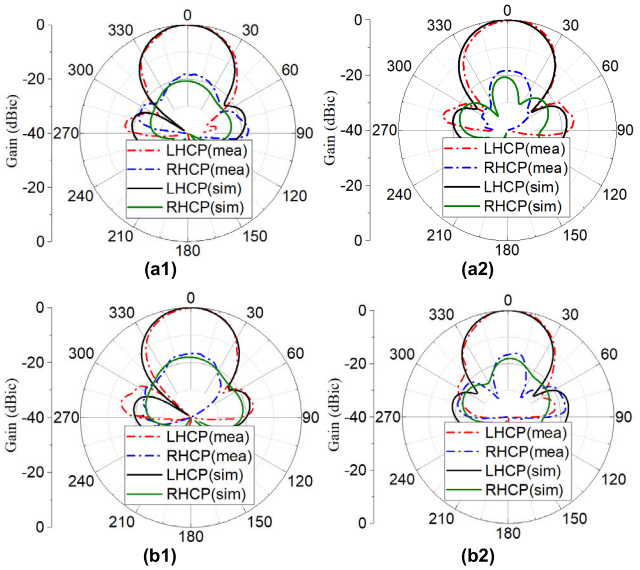

FIGURE 17. Simulated and measured radiation patterns of CP multilayer antenna array. (a1) *YOZ*-plane at 3.6 GHz, (a2) *XOZ*-plane at 3.6GHz (b1) *YOZ*-plane at 3.65GHz, (b2) *XOZ*-plane at 3.65GHz.

reach 140 MHz (3.54 GHz to 3.68 GHz). Fig. 16 shows the photograph seen from the top and back view of the printed CP antenna array. The simulated and measured radiation patterns of the CP multi-layer antenna array at 3.6 and 3.65 GHz in the *YOZ*-plane and *XOZ*-plane are presented in Figs. 17a and 17b, respectively.

VI. CONCLUSION

In this paper, a dielectric and conductor 3D printing system is used for the development of multi-modes patch antennas, where a surface-driven patch and embedded stacked patch are co-designed. An embedded transmission line is investigated for loss analysis and performance verification. The characterization of the dielectric properties is investigated for the desired frequency region. A bandwidth improvement thanks to multi-mode stacked patches can be achieved, taking advantage of the three-dimensional design capability, without requiring an additional substrate or affecting the in-plane dimensions of the prototype. Adjustable bandwidth and central frequency can be realized by tuning the width of driven and stacked patches. After that, multi-layer CP antennas, as well as LP and CP antenna arrays, are designed and fabricated. Feeding networks are printed under the ground layer, improving the flexibility of the design and helping to reduce the footprint of the arrays. The successful development of the multi-layer and multi-mode patch antennas using AME technology proves that a low-cost, high-performance, time-saving manufacturing technique can be a revolutionary approach for the upcoming 5G consumer mobile electronics.

REFERENCES

[1] M. D'Auria, W. J. Otter, J. Hazell, B. T. W. Gillatt, C. Long-Collins, N. M. Ridler, and S. Lucyszyn, "3-D printed metal-pipe rectangular waveguides," *IEEE Trans. Compon., Packag., Manuf. Technol.*, vol. 5, no. 9, pp. 1339–1349, Sep. 2015.

[2] P. Nayeri, M. Liang, R. A. Sabory-Garciá, M. Tuo, F. Yang, M. Gehm, H. Xin, and A. Z. Elsherbeni, "3D printed dielectric reflectarrays: Low-cost high-gain antennas at sub-millimeter waves," *IEEE Trans. Antennas Propag.*, vol. 62, no. 4, pp. 2000–2007, Oct. 2014.

[3] B. Li, P. F. Jing, L. Q. Sun, K. W. Leung, and X. Lv, "3D printed OAM reflectarray using half-wavelength rectangular dielectric element," *IEEE Access*, vol. 8, pp. 142892–142899, 2020.

[4] J. Zhu, Y. Yang, D. McGloin, R. Rajasekharan Unnithan, S. Li, S. Liao, and Q. Xue, "3-D printed planar dielectric linear-to-circular polarization conversion and beam-shaping lenses using coding polarizer," *IEEE Trans. Antennas Propag.*, vol. 68, no. 6, pp. 4332–4343, Jun. 2020.

[5] A. Massaccesi, P. Pirinoli, V. Bertana, G. Scordo, S. L. Marasso, M. Cocuzza, and G. Dassano, "3D-printable dielectric transmitarray with enhanced bandwidth at millimeter-waves," *IEEE Access*, vol. 6, pp. 46407–46418, 2018.

[6] B. Sanz-Izquierdo and E. A. Parker, "3-D printing of elements in frequency selective arrays," *IEEE Trans. Antennas Propag.*, vol. 62, no. 12, pp. 6060–6066, Dec. 2014.

[7] A. Shastri, B. Sanz-Izquierdo, E. A. Parker, S. Gao, P. Reynaert, Z. Chen, and L. Winchester, "3D printing of millimetre wave and low-terahertz frequency selective surfaces using aerosol jet technology," *IEEE Access*, vol. 8, pp. 177341–177350, 2020.

[8] P. I. Deffenbaugh, T. M. Weller, and K. H. Church, "Fabrication and microwave characterization of 3-D printed transmission lines," *IEEE Microw. Wireless Compon. Lett.*, vol. 25, no. 12, pp. 823–825, Dec. 2015.

[9] F. Cai, Y.-H. Chang, K. Wang, C. Zhang, B. Wang, and J. Papapolymerou, "Low-loss 3-D multilayer transmission lines and interconnects fabricated by additive manufacturing technologies," *IEEE Trans. Microw. Theory Techn.*, vol. 64, no. 10, pp. 3208–3216, Oct. 2016.

[10] A. Vallecchi, D. Cadman, W. G. Whittow, J. Vardaxoglou, E. Shamonina, and C. J. Stevens, "3-D printed bandpass filters with coupled vertically extruded split ring resonators," *IEEE Trans. Microw. Theory Techn.*, vol. 67, no. 11, pp. 4341–4352, Nov. 2019.

[11] A. Chauraya, J. Tudor, J. C. Vardaxoglou, R. Torah, Y. Li, W. G. Whittow, S. Beeby, and K. Yang, "Inkjet printed dipole antennas on textiles for wearable communications," *IET Microw., Antennas Propag.*, vol. 7, no. 9, pp. 760–767, Jun. 2013.
[12] B. S. Cook and A. Shamim, "Inkjet printing of novel wideband and high gain antennas on low-cost paper substrate," *IEEE Trans. Antennas Propag.*, vol. 60, no. 9, pp. 4148–4156, Sep. 2012.
[13] S. Hong, Y. Kim, and C. W. Jung, "Transparent microstrip patch antennas with multilayer and metal-mesh films," *IEEE Antennas Wireless Propag. Lett.*, vol. 16, pp. 772–775, 2017.
[14] S. Kim, Y.-J. Ren, H. Lee, A. Rida, S. Nikolaou, and M. M. Tentzeris, "Monopole antenna with inkjet-printed EBG array on paper substrate for wearable applications," *IEEE Antennas Wireless Propag. Lett.*, vol. 11, pp. 663–666, Jun. 2012.
[15] L. Catarinucci, F. P. Chietera, and R. Colella, "Permittivity-customizable ceramic-doped silicone substrates shaped with 3-D-printed molds to design flexible and conformal antennas," *IEEE Trans. Antennas Propag.*, vol. 68, no. 6, pp. 4967–4972, Jun. 2020.
[16] G. Muntoni, G. Montisci, G. A. Casula, F. P. Chietera, A. Michel, R. Colella, L. Catarinucci, and G. Mazzarella, "A curved 3-D printed microstrip patch antenna layout for bandwidth enhancement and size reduction," *IEEE Antennas Wireless Propag. Lett.*, vol. 19, no. 7, pp. 1118–1122, Jul. 2020.
[17] X. Yu, M. Liang, C. Shemelya, D. A. Roberson, R. Wicker, E. MacDonald, and H. Xin, "3-D printed parts for a multi-layer phased array antenna system," *IEEE Antennas Wireless Propag. Lett.*, vol. 17, no. 11, pp. 2150–2154, Nov. 2018.
[18] V. M. Pepino, A. F. da Mota, A. Martins, and B.-H.-V. Borges, "3-D-printed dielectric metasurfaces for antenna gain improvement in the Ka-band," *IEEE Antennas Wireless Propag. Lett.*, vol. 17, no. 11, pp. 2133–2136, Nov. 2018.
[19] M. F. Farooqui and A. Kishk, "3-D-printed tunable circularly polarized microstrip patch antenna," *IEEE Antennas Wireless Propag. Lett.*, vol. 18, no. 7, pp. 1429–1432, Jul. 2019.
[20] M. Liang, C. Shemelya, E. MacDonald, R. Wicker, and H. Xin, "3-D printed microwave patch antenna via fused deposition method and ultrasonic wire mesh embedding technique," *IEEE Antennas Wireless Propag. Lett.*, vol. 14, pp. 1346–1349, 2015.
[21] S. Wang, L. Zhu, and W. Wu, "3-D printed inhomogeneous substrate and superstrate for application in dual-band and dual-CP stacked patch antenna," *IEEE Trans. Antennas Propag.*, vol. 66, no. 5, pp. 2236–2244, May 2018.
[22] G. McKerricher, D. Titterington, and A. Shamim, "A fully inkjet-printed 3-D honeycomb-inspired patch antenna," *IEEE Antennas Wireless Propag. Lett.*, vol. 15, pp. 544–547, 2016.
[23] T. Bhattacharjee, H. Jiang, and N. Behdad, "A fluidically tunable, dual-band patch antenna with closely spaced bands of operation," *IEEE Antennas Wireless Propag. Lett.*, vol. 15, pp. 118–121, 2016.
[24] J. Sun and K.-M. Luk, "A circularly polarized water patch antenna," *IEEE Antennas Wireless Propag. Lett.*, vol. 19, no. 6, pp. 926–929, Jun. 2020.
[25] S. Wang, X. Zhang, L. Zhu, and W. Wu, "Single-fed wide-beamwidth circularly polarized patch antenna using dual-function 3-D printed substrate," *IEEE Antennas Wireless Propag. Lett.*, vol. 17, no. 4, pp. 649–653, Apr. 2018.
[26] K. X. Wang and H. Wong, "A wideband millimeter-wave circularly polarized antenna with 3-D printed polarizer," *IEEE Trans. Antennas Propag.*, vol. 65, no. 3, pp. 1038–1046, Mar. 2017.
[27] V. Bharambe, D. P. Parekh, C. Ladd, K. Moussa, M. D. Dickey, and J. J. Adams, "Liquid-metal-filled 3-D antenna array structure with an integrated feeding network," *IEEE Antennas Wireless Propag. Lett.*, vol. 17, no. 5, pp. 739–742, May 2018.
[28] L. Song, W. Gao, and Y. Rahmat-Samii, "3-D printed microfluidics channelizing liquid metal for multipolarization reconfigurable extended E-shaped patch antenna," *IEEE Trans. Antennas Propag.*, vol. 68, no. 10, pp. 6867–6878, Oct. 2020.
[29] S. Moscato, R. Bahr, T. Le, M. Pasian, M. Bozzi, L. Perregrini, and M. M. Tentzeris, "Infill-dependent 3-D-printed material based on NinjaFlex filament for antenna applications," *IEEE Antennas Wireless Propag. Lett.*, vol. 15, pp. 1506–1509, 2016.
[30] S. Narke, S. Ananthakrishnan, and C. Bhattacharya, "Enhancement of axial ratio-beamwidth of X-band composite microstrip patch antenna with conical ground plane," *Electron. Lett.*, vol. 56, no. 9, pp. 419–421, Apr. 2020.
[31] S. Jun, B. Sanz-Izquierdo, J. Heirons, C. X. Mao, S. Gao, D. Bird, and A. McClelland, "Circular polarised antenna fabricated with low-cost 3D and inkjet printing equipment," *Electron. Lett.*, vol. 53, no. 6, pp. 370–371, Mar. 2017.
[32] S. M. Radha, G. Shin, P. Park, and I.-J. Yoon, "Realization of electrically small, low-profile quasi-isotropic antenna using 3D printing technology," *IEEE Access*, vol. 8, pp. 27067–27073, 2020.
[33] B. T. Malik, V. Doychinov, S. A. R. Zaidi, I. D. Robertson, and N. Somjit, "Antenna gain enhancement by using low-infill 3D-printed dielectric lens antennas," *IEEE Access*, vol. 7, pp. 102467–102476, 2019.
[34] S. Alkaraki, Y. Gao, S. Stremsdoerfer, E. Gayets, and C. G. Parini, "3D printed corrugated plate antennas with high aperture efficiency and high gain at X-band and Ka-band," *IEEE Access*, vol. 8, pp. 30643–30654, 2020.
[35] K. Johnson, M. Zemba, B. P. Conner, J. Walker, E. Burden, K. Rogers, K. R. Cwiok, E. Macdonald, and P. Cortes, "Digital manufacturing of pathologically-complex 3D printed antennas," *IEEE Access*, vol. 7, pp. 39378–39389, 2019.
[36] V. T. Bharambe, J. Ma, M. D. Dickey, and J. J. Adams, "Planar, multifunctional 3D printed antennas using liquid metal parasitics," *IEEE Access*, vol. 7, pp. 134245–134255, 2019.
[37] P. M. Njogu, B. Sanz-Izquierdo, S. Y. Jun, G. Kalman, S. Gao, A. Malas, and G. J. Gibbons, "Evaluation of planar inkjet-printed antennas on a low-cost origami flapping robot," *IEEE Access*, vol. 8, pp. 164103–164113, 2020.
[38] M. I. Magray, G. S. Karthikeya, K. Muzaffar, S. K. Koul, and A. H. Moon, "Wideband asymmetric coplanar strip fed antennas with pattern diversity for mmWave 5G base stations," *IEEE Access*, vol. 8, pp. 77482–77489, 2020.
[39] K. Y. Kapusuz, S. Lemey, A. Petrocchi, P. Demeester, D. Schreurs, and H. Rogier, "Polarization reconfigurable air-filled substrate integrated waveguide cavity-backed slot antenna," *IEEE Access*, vol. 7, pp. 102628–102643, 2019.
[40] S. Sarjoghian, M. H. Sagor, Y. Alfadhl, and X. Chen, "A 3D-printed high-dielectric filled elliptical double-ridged horn antenna for biomedical monitoring applications," *IEEE Access*, vol. 7, pp. 94977–94985, 2019.
[41] X. Y. Liu, Y. Zhu, W. Xie, G. H. Peng, and W. Wang, "Generation of plane spiral orbital angular momentum waves by microstrip Yagi antenna array," *IEEE Access*, vol. 8, pp. 175688–175696, 2020.
[42] B. Urasinska-Wojcik, N. Chilton, P. Todd, C. Elsworthy, M. Bates, G. Roberts, and G. J. Gibbons, "Integrated manufacture of polymer and conductive tracks for real-world applications," *Additive Manuf.*, vol. 29, Oct. 2019, Art. no. 100777.
[43] P. F. Flowers, C. Reyes, S. Ye, M. J. Kim, and B. J. Wiley, "3D printing electronic components and circuits with conductive thermoplastic filament," *Additive Manuf.*, vol. 18, pp. 156–163, Dec. 2017.
[44] A. C. Paolella, C. Corey, D. Foster, J. Desjardins, C. Smith, and L. Walters, "Broadband millimeter wave characterization of 3-D printed materials," in *IEEE MTT-S Int. Microw. Symp. Dig.*, Jun. 2018, pp. 1565–1568.

MENGZE LI (Student Member, IEEE) was born in Hunan, China, in 1994. She received the B.Eng. degree in electrical engineering and automation from Hunan University, Hunan, in 2015, and the M.Eng. degree in electronic field and microwave technology from Xiamen University, Xiamen, China, in 2018. She is currently pursuing the Ph.D. degree with the Faculty of Engineering and Information Technology, University of Technology Sydney, Australia. From 2017 to 2018, she was a Visiting Student with the Faculty of Engineering and Information Technology, University of Technology Sydney.

Her current research interests include microstrip filters, multiplexers, RFIC, and 3-D print technology.

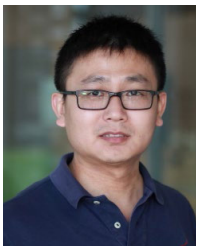

YANG YANG (Senior Member, IEEE) was born in Bayan Nur, Inner Mongolia, China. He received the M.Eng., M.Sc., and Ph.D. degrees from the Department of Electrical and Computer Systems Engineering, Monash University Clayton Campus, Melbourne, Australia, in 2007, 2008, and 2013, respectively.

He has three years industry experience at Rain Bird Australia serving as an Asia–Pacific GSP Engineer from 2012 to 2015. He received the corporate 2014 Global GSP Success Award (one globally). In 2015, he returned to academia and served as a Senior Research Associate with the Centre for Collaboration in Electromagnetic and Antenna Engineering, Macquarie University. In 2016, he was appointed as a Research Fellow with the State Key Laboratory of Terahertz and Millimeter Waves, The City University of Hong Kong. Since 2016, he has been with the University of Technology Sydney, Australia. He is currently a Senior Lecturer and a Team Leader of millimeter-wave integrated circuits and antennas. His research interests include millimeter-wave and sub-terahertz technologies in 5G and biomedical applications. He has over 150 international peer-reviewed publications in microwave and millimeter-wave circuits and antennas.

Dr. Yang is a currently a Committee Member of the MTT-28 Biological Effects and Medical Applications. He was a recipient of the CST University Publication Award 2018 from CST, Dassault Systèmes. He is a currently an Associate Editor of IEEE Access, and an Area Editor (Track Editor) of *Microwave and Optical Technology Letters*.

FRANCESCA IACOPI (Senior Member, IEEE) currently leads the Integrated Nanosystems Laboratory, Faculty of Engineering and Information Technology, University of Technology Sydney, and a Chief Investigator of the ARC Centre of Excellence in Transformative Meta-Optical Systems. She has over 20 years' international industrial and academic expertise in the miniaturization of semiconductor technologies. She has led large research and development projects for IMEC, Belgium, and GLOBALFOUNDRIES, Inc., USA, in interconnects, electronic devices, and packaging. Her focus is the translation of basic scientific advances into nanomaterials and device concepts into integrated technologies. She is known for her work in porous dielectrics for interconnects and graphene for on-chip applications. She is a Fellow of the Institution of Engineers Australia. She was a recipient of the MRS Gold Graduate Student Award in 2003, the ARC Future Fellowship in 2012, and the Global Innovation Award in Washington, DC, USA, in 2014. She currently serves in several technical committees for the Materials Research Society, the IEEE Electron Devices Society, and the International Roadmap for Systems and Devices. She was listed among the most innovative engineers by Engineers Australia in 2018.

JAIM NULMAN (Senior Member, IEEE) received the bachelor's degree in electrical engineering from the Technion-Israel Institute of Technology, the master's and Ph.D. degrees from Cornell University in electrical engineering, and the M.B.A. degree from Stanford University. He is a proven influencer and innovator with more than 30 years of expertise in working with companies from start-ups to fortune 500 enterprises. He served as the Vice President of applied materials, where he spent 15 years in several product division and corporate positions. He has served as an Invited Lecturer with the University of California at Berkeley, and the NATO's International Summer Institute. He drove the successful commercialization of one of applied materials' semiconductor manufacturing products with impressive market penetration of $1 billion in less than five years. He has a co-invented in over 30 patents in the area of semiconductor manufacturing technology, semiconductor manufacturing equipment, and additive manufacturing for electronics.

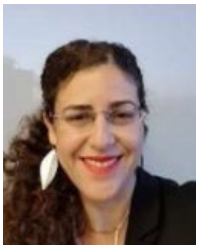

SHLOMIT CHAPPEL-RAM received the B.Sc. and Ph.D. degrees *(summa cum laude)* in chemistry and the M.B.A. degree from Bar-Ilan University. She has an extensive experience in research and development for the past 14 years, mostly from the medical devices industry, Edwards Lifesciences, and Medinol Ltd.

She is currently leading multi-disciplinary research and development teams, such as materials, formulations, chemistry, physics, process, mechanics, software, hardware, and electronics, in Nano-Dimension Technologies (Electrifying Additive Manufacturing company), from early phase needs throughout the development gates and to manufacturing transitions.